Multichannel High-Order Harmonic Generation from Fractal Bands in Fibonacci Quasicrystals

Jia-Qi Liu[1,2] and Xue-Bin Bian[1,*]

[1]State Key Laboratory of Magnetic Resonance and Atomic and Molecular Physics, Wuhan Institute of Physics and Mathematics, Innovation Academy for Precision Measurement Science and Technology, Chinese Academy of Sciences, Wuhan 430071, China
[2]School of Physical Sciences, University of Chinese Academy of Sciences, Beijing 100049, China

(Received 24 April 2021; revised 28 August 2021; accepted 20 October 2021; published 17 November 2021)

High-order harmonic generation (HHG) in solids was expected to be efficient due to their high density. However, the strict transition laws in crystals restrict the number of HHG channels. Quasicrystals with fractal band structures could solve this problem and produce multichannel HHG emissions, which has been rarely studied. We simulate the Fibonacci quasicrystal (FQ) HHG for the first time and investigate the electron dynamics on the attosecond timescale. Our results reveal that (i) the acceleration theorem is approximately applicable in FQ, which provides us a valuable tool to analyze the electron trajectories. (ii) Fractal bands lead to more excitation channels, analogous to the forbidden nonvertical electron transitions in crystals. (iii) The broken symmetry results in more frequent backscattering of electrons. (iv) Compared with crystals, multichannel HHG in FQ has a higher yield and wider spectral range. Our results pave the way to understand and control the HHG in quasicrystals and shed light on a potential shorter and stronger attosecond light source based on compact solids.

DOI: 10.1103/PhysRevLett.127.213901

High-order harmonic generation (HHG) in different materials driven by lasers has been investigated to produce coherent extreme ultraviolet sources [1] and ultrashort attosecond pulses [2]. Gas HHG has made considerable progress in the direction of wide spectral ranges for many years [3,4], and then crystal HHG has attracted much attention [5–11]. Recently, liquids have been also of great interest as a source of HHG [12,13] due to their fluidity and ubiquity. Condensed matters with a high density are expected to produce efficient HHG. However, the potential is not fully released because of many restrictions in the HHG processes. The vertical transition and recollision condition in crystal HHG exclude the contribution of many electrons [10]. The statistical effect in disordered liquid HHG leads to a finite coherence distance [13]. Quasicrystals are special ordered systems without translational periodicity [14,15]. Since the Bloch theorem or the statistical laws are not applicable to quasicrystals, the restrictions on HHG may be broken. To our knowledge, quasicrystals as one crucial kind of solid have not been studied to produce HHG.

Among many quasicrystal models, the one-dimensional (1D) Fibonacci quasicrystal (FQ) is relatively simple but has rich physical contents [15–18]. In 1985, Merlin *et al.* [19] made the first superlattice of FQ by using the molecular beam epitaxy method. Based on nonlinear optics, Feng *et al.* [20] theoretically analyzed the second-harmonic generation (SHG) and third-harmonic generation in FQ superlattices composed of $LiNbO_3$ crystals in 1990. Compared with the periodic structure, the 1D FQ system has more reciprocal lattice vectors, which is beneficial to the realization of quasi–phase matching. In 1997, Zhu *et al.* [21] realized the $LiTaO_3$ superlattice with a Fibonacci sequence and obtained the SHG of multiple center waves in experiments. Subsequently, the nonlinear optical effects of superlattices arranged according to other sequences have also been extensively studied [22–24]. However, the extreme nonlinear optical up-conversion HHG process in FQ has not been studied. The particular order of quasicrystals makes the essential difference from disordered (e.g., doped, amorphous) systems [25–27]. We will see that the dense reciprocal vectors of FQ result in frequent backscattering and significant wavelength dependence, which is different from HHG in disordered systems. Atomic units (a.u.) are used throughout unless stated otherwise.

To simulate FQ, we construct a 1D atomic chain. The arrangement of atomic spacing follows class A generalized Fibonacci model [GF$(m,1)$] [23,24] with a positive integer m. GF$(m,1)$ model is a quasiperiodic sequence obtained by a direct extension of the Fibonacci sequence (the rabbit problem), and its substitution rule is $B \to A$, $A \to A^m B$. As displayed in Fig. 1(a), from the high-dimensional projection method (HDPM) [28,29], the 1D quasicrystal can be obtained by the projection of the two-dimensional (2D) periodic lattice, with $\tan\theta$ is irrational. There are L_l (long) and L_s (short) two atomic spacings in the quasicrystal, as shown in Fig. 1(b). For the GF$(m,1)$ model, the angle θ should satisfy $\tan\theta = (1/\delta_m) = \{[\sqrt{m^2+4} - (2-m)]/2m\}$, where $\delta_m = 1 + (1/\tau_m) = [(\sqrt{m^2+4} + 2 - m)/2]$ and

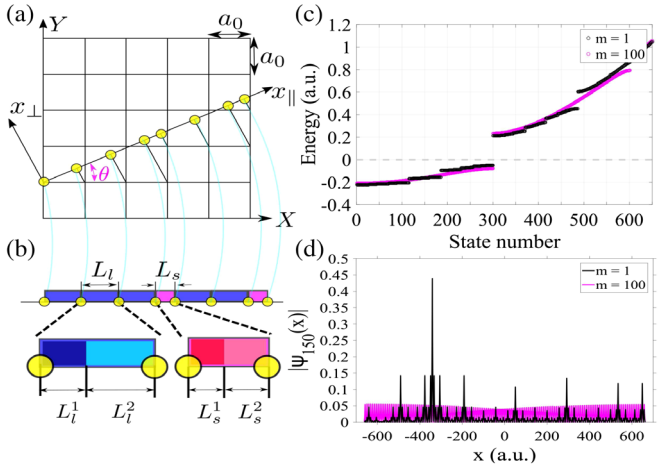

FIG. 1. (a) Schematic diagram of HDPM to obtain a 1D quasicrystal. θ is the angle between the vectors $x_{\parallel}$ and $\mathbf{X}$, controlling the sequence of atoms. (b) Schematic diagram of the 1D atomic chain based on HDPM. (c) Energy spectrum of FQ ($m = 1$, black circles) and the crystal ($m = 100$, magenta circles). The dashed gray line separates the valence band (VB) and conduction bands. (d) Modulus of the 150th eigenstate in FQ and the crystal.

$\tau_m = [(m + \sqrt{m^2+4})/2]$ [24]. The positions of atoms in the linear chain satisfy [15,23,24],

$$x_i = iL_s + (L_l - L_s)\left\lfloor \frac{i}{\delta_m} \right\rfloor, \qquad i \in [0, N-1], \quad (1)$$

where the symbol $\lfloor\rfloor$ stands for preserving the integer part. As manifested in Fig. 1(b), to satisfy $L_l/L_s = 1 + \tan\theta$ in HDPM, we set $L_s = L_s^1 + L_s^2$, $L_l = L_l^1 + L_l^2$, and make $L_s^1 = L_l^1 = l$, $L_s^2 = l(1 - \tau_m\eta)$, $L_l^2 = l(1+\eta)$, with $\eta = [2(\delta_m - 1)/(1 + \delta_m\tau_m)] = \{[(m+2)\sqrt{m^2+4} - m^2 - 2m - 2]/(2m+3)\}$ [20,21,24]. It is easy to know that $L_l/L_s = \delta_m$, $\delta_{m=1} = \tau_{m=1} = (\sqrt{5}+1)/2$, and as $m \to \infty$, $\delta_m \to 1$ ($\theta \to 45°$), therefore FQ ($m = 1$) is naturally related to the crystal ($m \to \infty$) by GF$(m, 1)$. Local Gaussian potentials are used to describe the Coulomb interaction between adjacent atoms $(x_i < x < x_{i+1})$ [13],

$$V_{\text{ion}}(x) = -V_0\left\{\exp\left[-\frac{(x-x_i)^2}{2\alpha^2}\right] + \exp\left[-\frac{(x-x_{i+1})^2}{2\alpha^2}\right]\right\}, \quad (2)$$

with $l = 2.2$ a.u., $V_0 = 0.8$ a.u., $\alpha = 0.16l$, and $N = 300$. The potentials are nearly independent of each other. It is similar to the off-diagonal FQ model [18] (in 1D tight-binding approximation) where the electron energy spectrum is a singularly continuous Cantor set and the eigenstates are self-similar (fractal) or chaotic critical wave functions [16–18], neither localized nor extended in a standard fashion.

The electron energy spectra of $m = 1$ (FQ) and $m = 100$ (crystal) are given in Fig. 1(c) by diagonalizing the field-free Hamiltonian. The energy bands in FQ have a three-split fractal structure similar to the off-diagonal model. All eigenstates with negative energies are occupied valence states. Figure 1(d) demonstrates the spatial distribution of the 150th eigenstate in the FQ and crystal, and the former is a fractal wave function [16,18]. We refer to the eigenstate with critical wave function as the critical state, and the criticality has been verified by calculating the multifractal dimension [30], as shown in Fig. S1 of Supplemental Material [31].

The interaction between the laser and FQ is simulated by solving the time-dependent Schrödinger equation. Similar to the time-dependent density functional theory with frozen Kohn-Sham potentials [26,33–35], all valence states ($i \le N$) are selected as initial states and evolve independently. The total current is $J(t) = \sum_i^N \int dx j_i(x,t)$, with $j_i(x,t) = -i[\psi_i^*(x,t)\partial_x\psi_i(x,t) - \psi_i(x,t)\partial_x\psi_i^*(x,t)]/2$. The harmonic spectrum is obtained by the Fourier transform of $J(t)$. The laser field is $E(t) = E_0 f(t)\cos(\omega t)$, with $E_0 = 0.0069$ a.u. The total duration L_t is 10 optical cycles (o.c.) with a trapezoidal envelope $f(t)$, including two rising and two falling cycles. The vector potential $A(t) = -\int dt E(t)$, with the amplitude $A_0 = E_0/\omega$. The open boundary condition is used, including vacuum regions (where the Coulomb potential is 0) at both ends of the linear chain. A $\cos^{1/8}$ function is adopted to absorb the reflection near the boundary.

Figure 2(a) shows the HHGs of FQ ($m = 1$) and crystal ($m = 100$) when the wavelength $\lambda = 0.5$ μm. It can be seen that the HHG in FQ with a cutoff of 15th order has a wider energy spectrum and a higher intensity than it does in the crystal with a cutoff of seventh order. We will explain in the following discussion that the extension of cutoff and the

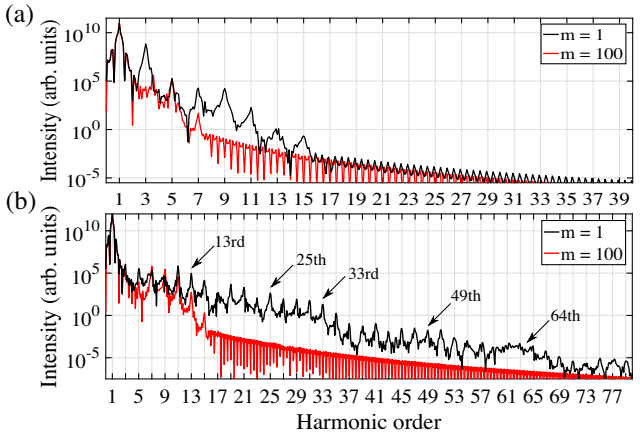

FIG. 2. Numerical results of HHG in FQ ($m = 1$) and crystal ($m = 100$). The wavelength λ is 0.5 and 1 μm in (a) and (b), respectively. In (b), the black arrows are the cutoff positions predicted by our theory. Other laser parameters are shown in the text.

enhancement above seventh order in FQ come from the more excitation channels. In Fig. 2(b), HHGs of FQ and crystal for $\lambda = 1$ μm are drawn. The increase of wavelength has little effect on the harmonic intensity and cutoff energy in the crystal. However, it has greatly changed the structure of the harmonic spectrum in FQ, and the most significant characteristic is the emergence of a multiplateau structure. We will see that more plateaus are caused by the backscattering. As shown in Fig. 1(c), the direct band gap of FQ is slightly smaller than that of crystal. We have verified that it does not affect our conclusion, except the third (fifth) order harmonic enhancement for $\lambda = 0.5(1)$ μm. More details can be found in the Supplemental Material [31].

Previous research [7–11,35–37] on crystal HHG illustrates that it comes from the intraband currents and interband polarizations. It inspires us to study the mechanism of FQ HHG in reciprocal space. The positions of reciprocal lattice sites (or Bragg peaks) in GF$(m, 1)$ quasicrystal are

$$G_{pq} = \frac{2\pi}{D}\left(p + \frac{q}{\delta_m}\right), \qquad p, q \in Z, \tag{3}$$

which corresponds to the Fourier transform of atomic positions [determined by Eq. (1)] [15,23,24], and $D = L_s + (L_l - L_s)/\delta_m$. Similar to the method in Refs. [26,33,35], the eigenstates were Fourier transformed from position to k space, and the modulus was plotted as a linear scaled contour plot vs k and the eigenvalue to get the energy bands of the FQ and crystals, as displayed in Figs. 3(a) and 3(b),

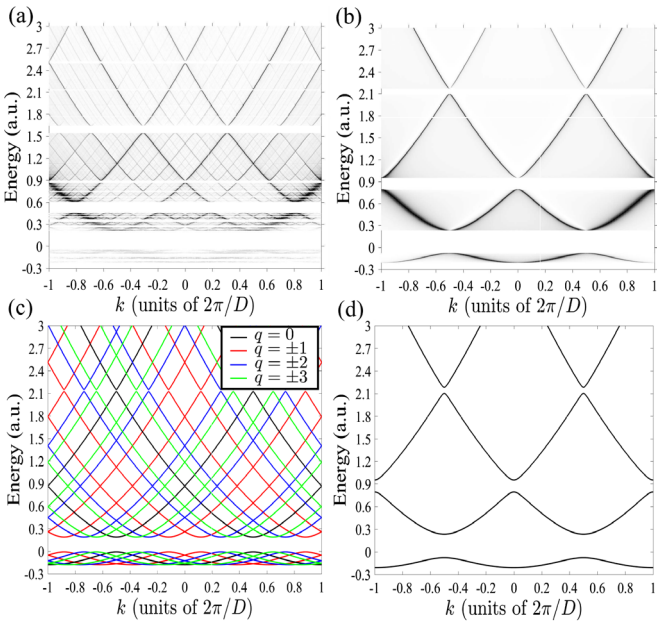

FIG. 3. Band structures of (a) FQ ($m = 1$) and (b) crystal ($m = 100$) in k space. (c) EC band (solid black line, $q = 0$) and (d) crystal band are calculated by PWEM. In (c), we translate the EC band by Eq. (3) with $p \in [-40, 40]$ and $q = \pm 1, \pm 2, \pm 3$ to reconstruct the FQ band.

respectively. A more extended discussion of this method can be found in Supplemental Material [31]. In crystals, the crystal momentum k is the quantum number of the translation operator's eigenvalue, and equivalent to the Fourier transformed momentum of eigenstates [26,33,35]. As mentioned in the Refs. [38–40], the quasicrystals have "modified" Bloch states, $\psi_k(x) = f_k(x)e^{ikx}$, which will be called quasi-Bloch states. $f_k(x)$ and $V_{\text{ion}}(x)$ are quasiperiodic functions [39,40], which can be expanded by the dense reciprocal lattice vectors. Based on the quasi-Bloch state, it is proved that the plane wave expansion method (PWEM) of crystals [41] can be extended to the calculation of FQ's band, and the results are in good agreement with Fig. 3(a) (see Fig. S2 and more details in Supplemental Material [31]). For FQ, k is the wave vector of the quasi-Bloch state, defined as the quasicrystal momentum, which is equivalent to the Fourier transformed momentum of eigenstates. From Figs. 1(d) and S1 (in the Supplemental Material [31]), most of the eigenstates in FQ (except a few edge states) are critical and extended states. Both of them are distributed in the whole space, but the former is more strongly modulated locally, which leads to multiple peaks in momentum space, as shown in Fig. S4(b) of the Supplemental Material [31]. Under the laser field, we find that these peaks in the k space obey something like the acceleration theorem [Figs. S4(c), S5, and S6 [31]]. Since the quasi-Bloch state in FQ has the same form as the Bloch state in crystals, we theoretically prove that the acceleration theorem in crystals can be approximately extended to our FQ model, based on the continuous band approximation. For details of derivation, please refer to the Supplemental Material [31].

In Fig. 3(a), it can be seen that the energy band of FQ has a very novel structure. From the perspective of energy, it is divided by many small gaps and forms the fractal structure, consistent with Fig. 1(c). These gaps fold the bands and lead to the translational band structure in the horizontal k space. Next, we try to reconstruct the FQ band from an effective-crystal (EC), whose periodic atomic potential comes from the spatial average of FQ's $V_{\text{ion}}(x)$ [31], to reduce the complexity and extract the electron dynamics information. From Eq. (3), the reciprocal lattice vector of GF$(m, 1)$ quasicrystal can be thought of as two parts: (i) $G_p = 2\pi/Dp$, representing the reciprocal lattice vectors of the EC with lattice constant D; (ii) $G_q = 2\pi/(D\delta_m)q$ implying that the reciprocal lattice vectors in (i) will be shifted by an integer multiple of $\Delta G_q = 2\pi/(D\delta_m)$, which corresponds to the translation of energy bands and Brillouin zone (BZ), consistent with translational band structure in Fig. 3(a). We calculated the energy band structures of EC and crystal by PWEM [41], as shown by the solid black lines in Figs. 3(c) and 3(d), respectively. In Fig. 3(c), the EC band ($q = 0$), has been shifted by Eq. (3) to reconstruct the FQ band. Both the fractal (energy space) and the translational (k space) structures are the results of the broken translational periodicity. The latter can

be perfectly reproduced by shifted EC bands and Eq. (3) (see Fig. S7 and more details in Supplemental Material [31]), while the former cannot.

As demonstrated in Fig. 4(b), in crystals, the excitation rate is high around the minimum band gap (black arrow 1), while it is small at large gaps (black arrow 3). And nonvertical transitions cannot occur (black arrow 2) without considering lattice vibration. The translational band structure in FQ causes more electron excitation channels, as marked by the black arrows in Fig. 4(a). Since FQ bands can be thought of as a series of shifted EC bands with $\Delta k = 2\pi/(D\delta_m)q$, q can be used as an indicator to describe different EC bands. $E^v_{q_1}(k_0)$ and $E^c_{q_2}(k_0)$ represent the energy of electrons before and after vertical excitation at k_0. When $q_1 = q_2$, the transition is like it in crystals (black arrow 1). $q_1 \neq q_2$ leads to more excitation paths (black arrows $2 \sim 4$), and $E^c_{q_1}(k_0) \neq E^c_{q_2}(k_0)$. In the latter case, we can always find the energy $E^c_{q_2}(k_0)$ in the initial EC band, that is, $E^c_{q_1}(k') = E^c_{q_2}(k_0)$ and $k' \neq k_0$, analogous to a nonvertical transition in the crystal. In Fig. 2(a), $A_0 = 0.0718$ a.u. is very small, and the backscattering is very weak (discussed later). More excitation channels in FQ will help more electrons participate in the harmonic radiation and extend the harmonic cutoff. To prove this, the highest occupied state has been taken as the initial state, whose time-dependent electron population (TDEP) is calculated by projecting the time-dependent wave function onto all the eigenstates at each moment. The energy-resolved TDEP is displayed in Figs. 4(c) and 4(e). In Fig. 4(c), after the electric field starts, some electrons are excited directly to higher bands and then driven by the field. In Fig. 4(d), the vertical brown dotted lines are draw on the FQ band to mark the vertical transitions of the highest valence electron. The ordinate of the intersections of above dotted lines and shifted EC bands correspond to the energy of the directly excited electrons in Fig. 4(c). The purple horizontal dotted lines are used to guide the eye. It proves that our conclusion is correct.

In crystals, backscattering occurs only at high symmetry points. In Fig. 4(b), the blue arrows ① and ② represent the k-space electron trajectories in two adjacent 1/4 o.c., without backscattering. The backscattering occurs at the BZ boundary (points p_1 or p_2), and the trajectories after

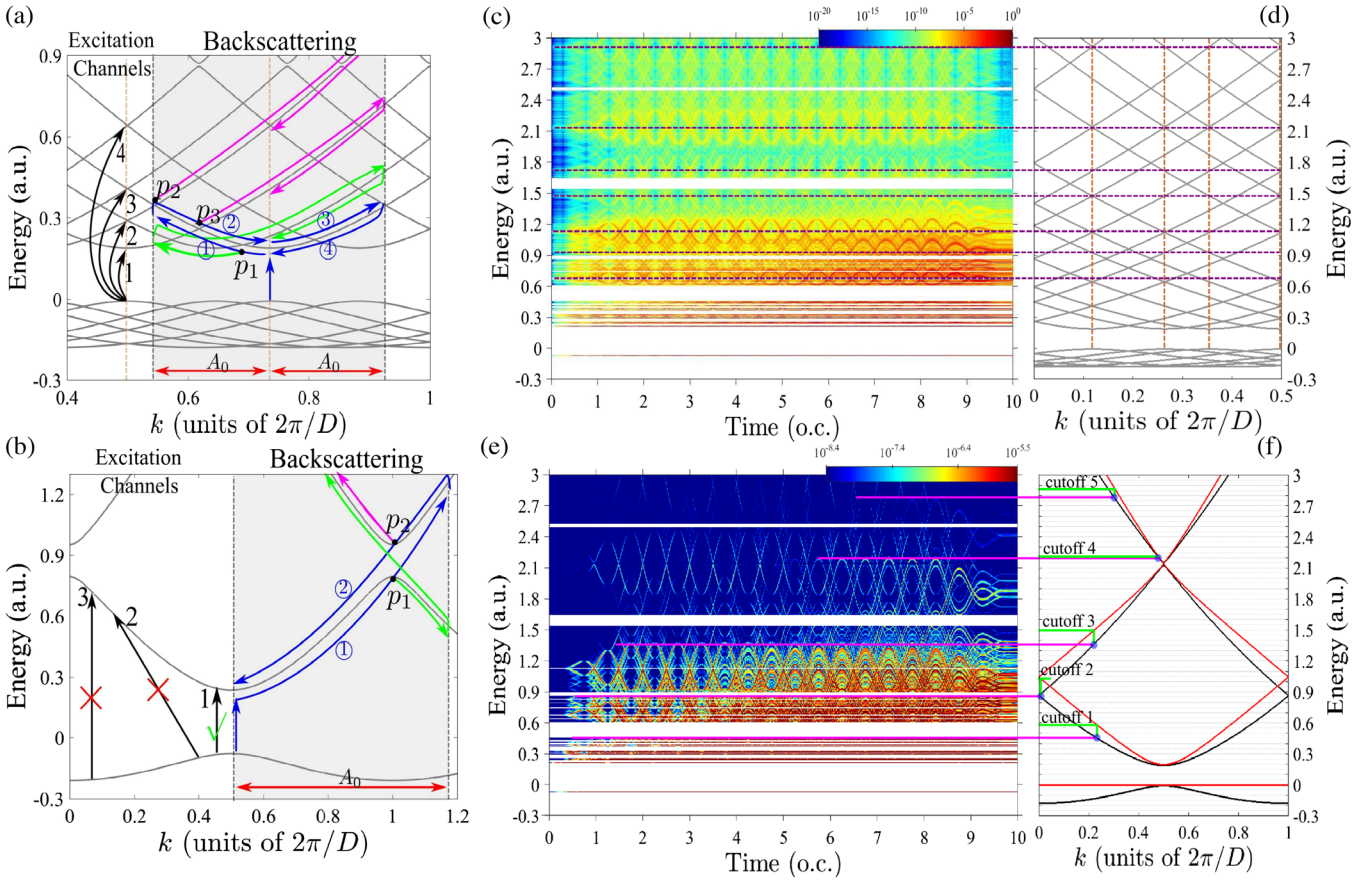

FIG. 4. (a) and (b) Schematic diagrams of electron excitation channels and backscattering of FQ and crystals in k space, respectively. The bands come from Figs. 3(c) and 3(d). The energy-resolved TDEP is displayed for (c) $\lambda = 0.5$ μm and (e) $\lambda = 1$ μm, respectively, taking the highest valance state as the initial state. (d) The band is the same as it is in Fig. 3(c), and the brown dotted lines mark the vertical transition of the highest valence electron. (f) EC band and its band gap between all bands and VB are drawn in solid black and red lines, respectively.

backscattering are displayed by the green and magenta arrows. A_0 is required to be large enough to make the electron reach BZ boundaries. Unlike crystals, the translational band structure of FQ causes frequent backscattering without large A_0 requirement. Figure 4(a) shows the k-space electron trajectories of FQ. The blue arrows ①∼④ manifest the electron movement on a EC band in one cycle. Some trajectories after backscattering are displayed with green and magenta arrows. In the first half cycle, electrons are scattered at p_1, p_2, and p_3 in turn and then driven by the field. Compared with the trajectories of backscattering at p_2 and p_3, the former can obtain higher photon energy, so A_0 can significantly affect HHG by backscattering. To verify the contribution of backscattering, we also calculated the energy-resolved TDEP of the highest valance electron in FQ, as exhibited in Fig. 4(e), with $\lambda = 1$ μm. In addition to the direct excitation channels, the energy-resolved TDEP accumulates with time in some energy range, such as $0.6 \sim 1.5$ a.u. or $1.6 \sim 2.1$ a.u., which comes from frequent backscattering.

Next, we extract the harmonic cutoff from energy-resolved TDEP. Figure 4(f) displays the EC band and its vertical gap between each band and VB in the solid black and red lines, respectively. The magenta horizontal lines project the maximum energy of different electron paths in Fig. 4(e) to the EC band in Fig. 4(f) and give the projection points. The green polylines assign the above projection points to the band gap at the same k, and the band gap energies correspond to the cutoffs. As shown in Fig. 4(f), cutoff 1 = 0.6 a.u. (13.17ω), cutoff 2 = 1.15 a.u. (25.2ω), cutoff 3 = 1.48 a.u. (32.5ω), cutoff 4 = 2.2 a.u. (48.3ω), and cutoff 5 = 2.9 a.u. (63.6ω), with $\lambda = 1$ μm. We correspond the above cutoffs to the harmonic spectrum in Fig. 2(b), as manifested by the black arrows, which are qualitatively consistent with the results of the time-dependent Schrödinger equation. Therefore, multiplateau structure of FQ HHG in Fig. 2(b) is the result of backscattering. And multiexcitation channels and backscattering together contribute to the harmonic emission before the 33rd order, while backscattering mainly contributes to the higher harmonics order.

In conclusion, to our knowledge, the mechanism of HHG in FQ is studied for the first time. We find that the band theory is approximately valid for FQ HHG, and the fractal band leads to more excitation channels and frequent backscattering. The former could enhance harmonic yield by orders and extend the cutoff obviously, while the latter makes the multiplateau structure of HHG. Our Letter elucidates the ultrafast electron dynamics in laser-quasicrystal interactions and opens the possibility of detecting novel electronic properties (such as band structure) of quasicrystals by all-optical means in strong-field physics. Compared with crystals, FQs have the advantages of producing HHG with higher intensity and wider spectrum, so we expect that our work could push forward the efficient and compact HHG sources in condensed matters.

We thank Professor X. W. Guan, Professor X. M. Cai, and Professor M. H. Yuan for helpful discussions. This work is supported by the National Key Research and Development Program of China (No. 2019YFA0307702), the National Natural Science Foundation of China (No. 91850121), and the K. C. Wong Education Foundation (GJTD-2019-15).

*xuebin.bian@wipm.ac.cn

[1] J. J. Macklin, J. D. Kmetec, and C. L. Gordon, Phys. Rev. Lett. **70**, 766 (1993).
[2] P. M. Paul, E. S. Toma, P. Breger, G. Mullot, F. Augé, Ph. Balcou, H. G. Muller, and P. Agostini, Science **292**, 1689 (2001).
[3] A. McPherson, G. Gibson, H. Jara, U. Johann, T. S. Luk, I. A. McIntyre, K. Boyer, and C. K. Rhodes, J. Opt. Soc. Am. B **4**, 595 (1987).
[4] P. B. Corkum, Phys. Rev. Lett. **71**, 1994 (1993).
[5] K. A. Pronin, A. D. Bandrauk, and A. A. Ovchinnikov, Phys. Rev. B **50**, 3473 (1994).
[6] A. H. Chin, O. G. Calderón, and J. Kono, Phys. Rev. Lett. **86**, 3292 (2001).
[7] D. Golde, T. Meier, and S. W. Koch, Phys. Rev. B **77**, 075330 (2008).
[8] S. Ghimire, A. D. Dichiara, E. Sistrunk, P. Agostini, L. F. Dimauro, and D. A. Reis, Nat. Phys. **7**, 138 (2011).
[9] O. Schubert, M. Hohenleutner, F. Langer, B. Urbanek, C. Lange, U. Huttner, D. Golde, T. Meier, M. Kira, S. W. Koch, and R. Huber, Nat. Photonics **8**, 119 (2014).
[10] G. Vampa, C. R. McDonald, G. Orlando, D. D. Klug, P. B. Corkum, and T. Brabec, Phys. Rev. Lett. **113**, 073901 (2014).
[11] F. Langer, C. P. Schmid, S. Schlauderer, M. Gmitra, J. Fabian, P. Nagler, C. Schüller, T. Korn, P. G. Hawkins, J. T. Steiner, U. Huttner, S. W. Koch, M. Kira, and R. Huber, Nature (London) **557**, 76 (2018).
[12] T. T. Luu, Z. Yin, A. Jain, T. Gaumnitz, Y. Pertot, J. Ma, and H. J. Wörner, Nat. Commun. **9**, 3723 (2018).
[13] A. W. Zeng and X. B. Bian, Phys. Rev. Lett. **124**, 203901 (2020).
[14] D. Shechtman, I. Blech, D. Gratias, and J. W. Cahn, Phys. Rev. Lett. **53**, 1951 (1984).
[15] D. Levine and P. J. Steinhardt, Phys. Rev. B **34**, 596 (1986).
[16] Q. Niu and F. Nori, Phys. Rev. Lett. **57**, 2057 (1986).
[17] M. Kohmoto, L. P. Kadanoff, and C. Tang, Phys. Rev. Lett. **50**, 1870 (1983).
[18] M. Kohmoto, B. Sutherland, and C. Tang, Phys. Rev. B **35**, 1020 (1987).
[19] R. Merlin, K. Bajema, R. Clarke, F. Y. Juang, and P. K. Bhattacharya, Phys. Rev. Lett. **55**, 1768 (1985).
[20] J. Feng, Y. Y. Zhu, and N. B. Ming, Phys. Rev. B **41**, 5578 (1990).
[21] S. N. Zhu, Y. Y. Zhu, Y. Q. Qin, H. F. Wang, C. Z. Ge, and N. B. Ming, Phys. Rev. Lett. **78**, 2752 (1997).

[22] X. J. Liu, Z. L. Wang, X. S. Jiang, J. Wu, and N. Ming, J. Phys. D **31**, 2502 (1998).
[23] J. Birch, M. Severin, U. Wahlström, Y. Yamamoto, G. Radnoczi, R. Riklund, J. E. Sundgren, and L. R. Wallenberg, Phys. Rev. B **41**, 10398 (1990).
[24] Y. Chen, X. B. Yang, Q. Guo, and S. Lan, J. Phys. Condens. Matter **18**, 2587 (2006).
[25] T. Huang, X. Zhu, L. Li, X. Liu, P. Lan, and P. Lu, Phys. Rev. A **96**, 043425 (2017).
[26] C. Yu, K. K. Hansen, and L. B. Madsen, Phys. Rev. A **99**, 013435 (2019).
[27] P. Jürgens, B. Liewehr, B. Kruse, C. Peltz, D. Engel, A. Husakou, T. Witting, M. Ivanov, M. J. J. Vrakking, T. Fennel, and A. Mermillod-Blondin, Nat. Phys. **16**, 1035 (2020).
[28] V. Elser and C. L. Henley, Phys. Rev. Lett. **55**, 2883 (1985).
[29] V. Elser, Phys. Rev. B **32**, 4892 (1985).
[30] X. Cai, J. Phys. Condens. Matter **30**, 345601 (2018).
[31] See Supplemental Material at http://link.aps.org/supplemental/10.1103/PhysRevLett.127.213901 for additional information, which includes Ref. [32].
[32] S. Spurrier and N. R. Cooper, Phys. Rev. A **97**, 043603 (2018).
[33] D. Bauer and K. K. Hansen, Phys. Rev. Lett. **120**, 177401 (2018).
[34] N. Tancogne-Dejean, O. D. Mücke, F. X. Kärtner, and A. Rubio, Phys. Rev. Lett. **118**, 087403 (2017).
[35] C. Yu, H. Iravani, and L. B. Madsen, Phys. Rev. A **102**, 033105 (2020).
[36] J. Li, S. Fu, H. Wang, X. Zhang, B. Ding, B. Hu, and H. Du, Phys. Rev. A **98**, 043409 (2018).
[37] M. F. Ciappina *et al.*, Rep. Prog. Phys. **80**, 054401 (2017).
[38] E. Rotenberg, W. Theis, K. Horn, and P. Gille, Nature (London) **406**, 602 (2000).
[39] C. Janot, *Quasicrystals: A Primer* (Oxford University Press, New York, 1997).
[40] I. Blinov, Sci. Rep. **5**, 11492 (2015).
[41] M. Korbman, S. Y. Kruchinin, and V. S. Yakovlev, New J. Phys. **15**, 013006 (2013).